Practical issues in anisotropic full waveform inversion

Huy Le

ABSTRACT

In the previous report, SEP 163, I demonstrated the potential of using the second-order pseudo-acoustic anisotropic wave equations for full waveform inversion with simple examples. In this report, I investigate some practical issues that anisotropic full waveform inversion implemented with this system of equations faces. These issues are parameter sensitivity, parameterization, and null space. Firstly, to take into account differences in sensitivity of different anisotropic parameters, I suggest a simple normalization technique. This normalization results in dimensionless parameters that better reflect sensivity to recorded data. Secondly, a number of parameterizations, including stiffness coefficients, velocities, and Thomsen's parameters, are tested on the BP 2007 synthetic model. I found that parameterizations with one velocity and two Thomsen's parameters gave the best results in terms of reduction in the objective function. Lastly, to mitigate the null space problem, I regularize the inversion with steering filters based on the migrated image's dip information.

INTRODUCTION

Full waveform inversion (FWI) is a powerful technique to obtain both the long-wavelength (background) and the short-wavelength (reflectivity) components of a velocity model by minimizing the difference between the observed data and the modeled data. Successful applications of FWI generally require low-frequency and long-offset data, particularly diving waves, in order to solve the cycle skipping problem. When processing long-offset data, it is necessary to incorporate anisotropy to account for the dependence of seismic velocity on propagation direction. Studies have shown that FWI with anisotropy leads to better results (Barnes et al., 2008; Lee et al., 2010).

Anisotropic FWI poses more challenges compared to isotropic FWI. These challenges come from the increase in the number of unknown parameters. An anisotropic medium is characterized not only by velocity but also by anisotropic parameters that describe how velocity changes with direction. The first challenge is to account for different sensitivities, units, and magnitudes among these different parameters. The second challenge is to find a suitable parameterization. Multiple parameters are required for anisotropy and there are a number of equivalent sets of them. Another challenge in anisotropic FWI is the extension of the problem's null space, which is

a direct consequence of increasing number of parameters. In this report, I propose some solutions to these challenges.

Because the earth supports elastic wave motions, one will have to use elastic wave equations in order to handle the amplitude and kinematics of seismic waves. However, in the context of parameter estimation, a large number of unknowns in elastic FWI poses many difficulties, both theoretically and computationally. Consequently, acoustic wave equations have been commonly used and have shown successes in many FWI applications (Gholami et al., 2013b; Warner et al., 2013). Although acoustic anisotropy is not realistic, the resulting equations may accurately describe the kinematics of waves in anisotropic media. This work adopts a time-domain method that was developed by Le (2016) in the previous report for anisotropic FWI. This method is based on the second-order pseudo-acoustic wave equations in transverse isotropic media (VTI) (Duveneck and Bakker, 2011):

$$\begin{cases} \partial_t^2 p = c_{11}\partial_x^2 p + c_{13}\partial_z^2 q + f_x, \\ \partial_t^2 q = c_{13}\partial_x^2 p + c_{33}\partial_z^2 q + f_z. \end{cases} \tag{1}$$

p and q are the normal stresses in the x-direction and z-direction, f_i are the sources, and c_{ij} are the density-normalized stiffness coefficients.

Define $\mathbf{x}$ to be the location vector, $\mathbf{x}_r$ to be the receiver location, and $\mathbf{m}$ to be the vector of model parameters. The modeled pressure field is defined as the average stress, $d(\mathbf{x}, t; \mathbf{m}) = \frac{1}{2}(p + q)$. The FWI objective function can be defined as the l_2-norm of the difference between the modeled data and the observed data, $d_0(\mathbf{x}_r, t)$:

$$\chi(\mathbf{m}) = \frac{1}{2}\|d(\mathbf{x}_r, t; \mathbf{m}) - d_0(\mathbf{x}_r, t)\|_2^2. \tag{2}$$

Following the adjoint state method presented in Fichtner (2011), the gradients of the objective function with respect to model parameters are computed as cross-correlations of the adjoint wavefields, p_1 and q_1, and the forward modeling wavefields, p and q:

$$g_{c_{11}} = \int_0^T p_1 \partial_x^2 p dt, \tag{3a}$$

$$g_{c_{13}} = \int_0^T (p_1 \partial_z^2 q + q_1 \partial_x^2 p) dt, \tag{3b}$$

$$g_{c_{33}} = \int_0^T q_1 \partial_z^2 q dt. \tag{3c}$$

The adjoint wavefields are solutions to the adjoint equations:

$$\begin{cases} \partial_t^2 p_1 = \partial_x^2(c_{11}p_1 + c_{13}q_1) + \frac{1}{2}(d - d_0)\delta(\mathbf{x} - \mathbf{x_r}), \\ \partial_t^2 q_1 = \partial_z^2(c_{13}p_1 + c_{33}q_1) + \frac{1}{2}(d - d_0)\delta(\mathbf{x} - \mathbf{x_r}). \end{cases} \tag{4}$$

BALANCING THE GRADIENTS

There are several ways to parameterize the subsurface and the inversion problem. One common way is to use velocity and Thomsen's anisotropic parameters (Thomsen, 1986). The stiffness coefficients, c_{ij}, are related to vertical P-velocity, v_z, ϵ, and δ, by:

$$c_{11} = v_z^2(1+2\epsilon), \tag{5a}$$
$$c_{13} = v_z^2\sqrt{1+2\delta}, \tag{5b}$$
$$c_{33} = v_z^2. \tag{5c}$$

The gradients of the FWI objective function with respect to v_z, ϵ, and δ, can be easily computed from equations 3 by chain rules:

$$g_{v_z} = 2v_z(1+2\epsilon)g_{c_{11}} + 2v_z\sqrt{1+2\delta}g_{c_{13}} + 2v_z g_{c_{33}}, \tag{6a}$$
$$g_{\epsilon} = 2v_z^2(1+2\epsilon)g_{c_{11}}, \tag{6b}$$
$$g_{\delta} = \frac{v_z^2}{\sqrt{1+2\delta}}g_{c_{13}}. \tag{6c}$$

Because the stiffness coefficients, c_{ij}, have the same dimension, the same order of magnitude, and approximately equal sensitivity to the observed data (Gholami et al., 2013a), equations 3 can be used directly in a gradient-based optimization algorithm to minimize the objective function (Le, 2016). When parameterized with v_z, ϵ, and δ, these parameters not only have different dimensions and magnitudes, but also very different sensitivities, with v_z the most sensitive parameter. Its sensitivity is an order of magnitude larger than that of ϵ, which is in turn much larger than δ's. As a result, not accounting for these differences can lead to bad estimates of subsurface parameters.

I propose a simple normalization that can mitigate the differences in dimensions, magnitudes, and sensitivities among parameters such as v_z, ϵ, and δ. Instead of inverting for these parameters directly, I invert for a set of equivalent but normalized parameters, $\bar{v}_z$, $\bar{\epsilon}$, and $\bar{\delta}$ defined by:

$$\bar{v}_z = \frac{v_z}{v_0}, \bar{\epsilon} = \frac{\epsilon}{\epsilon_0}, \bar{\delta} = \frac{\delta}{\delta_0}. \tag{7}$$

The normalization coefficients, v_0, ϵ_0, and δ_0 are scalar constants chosen to satisfy:

$$\frac{g_{\bar{v}_z}}{\bar{v}_z} = \frac{g_{\bar{\epsilon}}}{\bar{\epsilon}} = \frac{g_{\bar{\delta}}}{\bar{\delta}}. \tag{8}$$

These equations promote approximately the same amount of update to all parameters at each inversion iteration.

I illustrate the improvement of this parameter normalization using a portion of the BP 2007 VTI synthetic model. Figure 1 shows the true model parameters and

Figure 2 shows the initial model parameters. The observed data is synthesized using the same engine as the modeled data with a Ricker wavelet of 5 Hz central frequency. 100 sources and 1600 receivers are placed uniformly on the water surface. Source spacing is 200 meters and receiver spacing is 12.5 meters. Maximum offset is 20 km.

Figure 3 shows the gradients with respect to unnormalized parameters, v_z, ϵ, and δ. Note from the scale bars that g_{v_z} (Figure 3(a)) is three orders of magnitude smaller than the other two gradients, g_ϵ (Figure 3(b)) and g_δ (Figure 3(c)). After normalization, $g_{\bar{v}_z}$ (Figure 4(a)) is now greater than $g_{\bar{\epsilon}}$ (Figure 4(b)), which is greater than $g_{\bar{\delta}}$ (Figure 4(c)). This means that the gradients with respect to normalized parameters better reflect their sensitivities to the data. Notice that because the normalization coefficients v_0, ϵ_0, and δ_0 are scalar constants, the change of variables from unnormalized to normalized does not change the geologic structures in the gradients, but only the magnitudes of their updates.

I performed two inversions with unnormalized and normalized parameters, and the results are shown in Figures 5 and 6 respectively. Compared with the true model (Figure 1), the inverted model using unnormalized parameters (Figure 5) shows unrealistic updates in ϵ and δ and almost no update in v_z. Inversion with normalized parameters (Figure 6) shows significant update in velocity, although updates in ϵ and δ are small. Figure 7 compares two objective functions from these inversions. Inversion with normalized parameters reduces the objective function much more than without normalization. In fact, without normalization, the inversion gets stuck after 13 iterations.

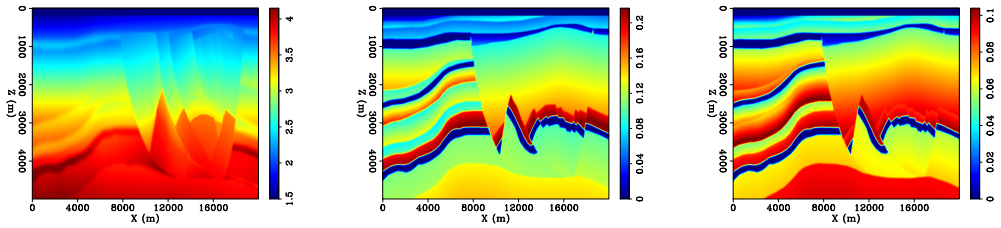

(a) (b) (c)

Figure 1: True model: (a) v_z in km/s, (b) ϵ, and (c) δ. [**ER**]

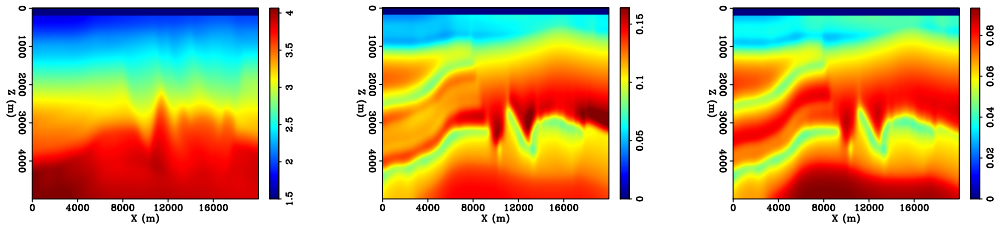

(a) (b) (c)

Figure 2: Initial model: (a) v_z in km/s, (b) ϵ, and (c) δ. [**ER**]

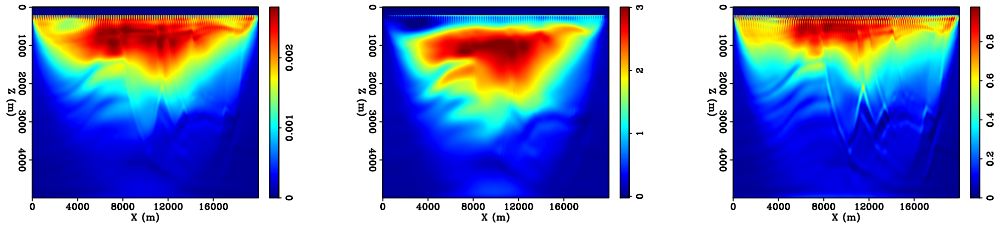

(a) (b) (c)

Figure 3: Gradients with respect to unnormalized parameters: (a) g_{v_z}, (b) g_ϵ, and (c) g_δ. Notice from the scale bars that g_{v_z} is three orders of magnitude smaller than the other two gradients. [**CR**]

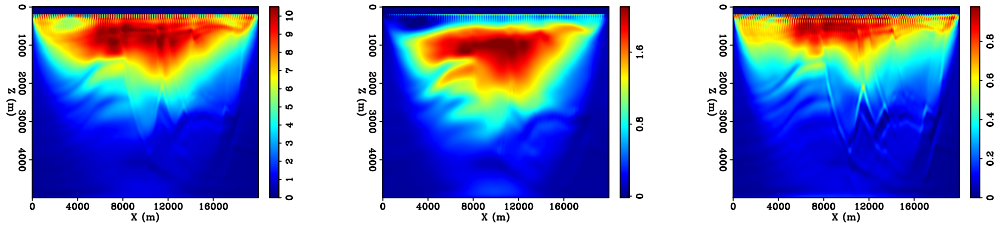

(a) (b) (c)

Figure 4: Gradients with respect to normalized parameters: (a) $g_{\bar{v}_z}$, (b) $g_{\bar{\epsilon}}$, and (c) $g_{\bar{\delta}}$. The scale bars show that these gradients more accurately reflect the sensitivities of unknown parameters. [**CR**]

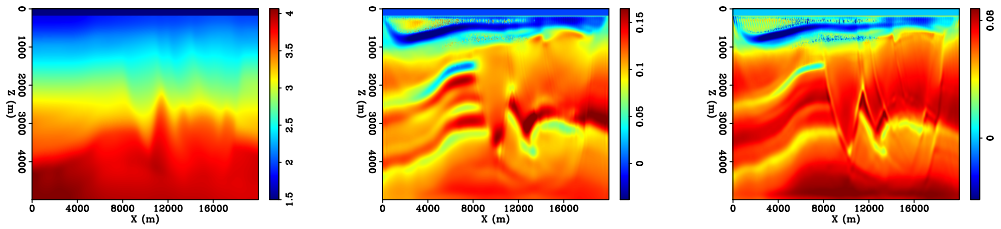

(a) (b) (c)

Figure 5: Inverted model using unnormalized parameters: (a) v_z in km/s, (b) ϵ, and (c) δ. Velocity is almost not updated while the other two parameters show unrealistic features. [**CR**]

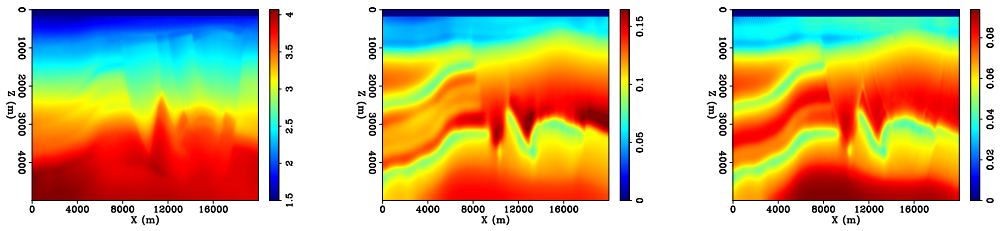

(a) (b) (c)

Figure 6: Inverted model using normalized parameters: (a) v_z in km/s, (b) ϵ, and (c) δ. Velocity is much better resolved compared to the inversion with unnormalized parameters, even though anisotropic parameters are weakly updated. [**CR**]

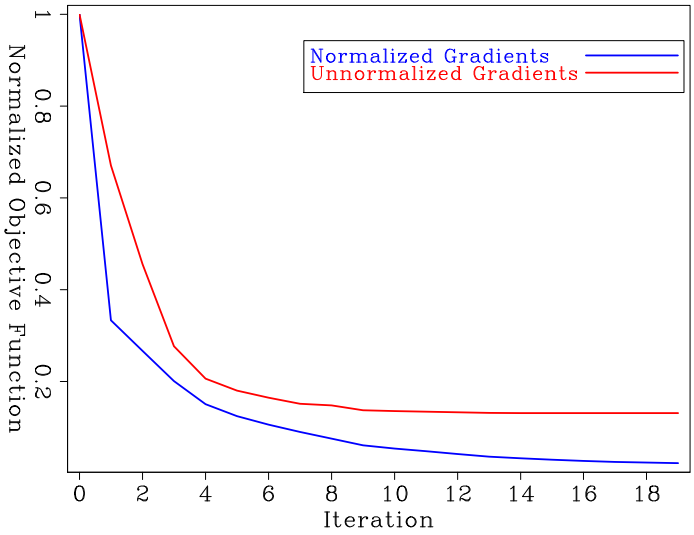

Figure 7: Comparison of objective functions from inversions with and without normalization. Inversion with normalized parameters does not get stuck and leads to a lower objective function. [**CR**]

PARAMETERIZATION TEST

Parameterization is a vital aspect of anisotropic FWI. A set of parameters that is most resolvable and has minimal trade-offs can lead to better inversion results. Besides stiffness coefficients c_{ij}, vertical velocity v_z, and Thomsen's parameters ϵ and δ, there are other parameters that also play an important role in describing anisotropic media. They are horizontal velocity v_h, normal moveout (NMO) velocity v_n, and the anellipticity parameter η:

$$v_h = v_z\sqrt{1+2\epsilon}, \tag{9a}$$

$$v_n = v_z\sqrt{1+2\delta}, \tag{9b}$$

$$\eta = \frac{\epsilon-\delta}{1+2\delta}. \tag{9c}$$

Many studies have been devoted to parameterization in anisotropic media. Alkhalifah and Tsvankin (1995) derive an expression for P-wave travel time in VTI media and show that it depends on two parameters: NMO velocity v_n and anellipticity parameter η. Plessix and Cao (2011) compute the eigenvalues of the Hessian of the FWI objective function and conclude that NMO and horizontal velocities are the most sensitive parameters. While NMO velocity is responsible for reflection events, horizontal velocity is responsible for diving waves and post-critical reflections. Gholami et al. (2013a) analyze and plot the radiation patterns of different sets of parameters to study sensitivity and trade-off.

In this work, I carry out several inversions using parameterizations that have been studied by Gholami et al. (2013a) in order to compare their performances. Four types of parameterizations are tested. The first type includes stiffness coefficients c_{ij}. The second type consists of three parameterizations with one velocity and two anisotropic parameters: $\{v_z, \epsilon, \delta\}$, $\{v_n, \eta, \delta\}$, and $\{v_h, \epsilon, \eta\}$. The third type has two velocities and one anisotropic parameter in two different sets: $\{v_z, v_h, \delta\}$ and $\{v_n, v_h, \delta\}$. The last type contains three velocities $\{v_z, v_n, v_h\}$. The inversions are run on the BP 2007 synthetic model with the same setting and acquisition as mentioned earlier. They start from the same initial model and the normalization technique described in the previous section is applied whenever unknown parameters are of different dimensions (the second and third types).

Figure 8 shows a comparison of objective functions from inversions with different parameterizations. I observe that the second type of parameterization with one velocity and two anisotropic parameters gave the best results in terms of reduction in objective function. Within this type, all three parameterizations, $\{v_z, \epsilon, \delta\}$, $\{v_n, \eta, \delta\}$, and $\{v_h, \epsilon, \eta\}$, perform equally well. The third type of parameterization with two velocities and one anisotropic parameter is second in performance while parameterizations with stiffness coefficients (the first type) and with three velocities (the fourth type) give roughly equally worst results.

Figures 10, 12, 14, 16, 18, 20, and 22 show updates of model parameters for seven tested parameterizations. These updates are to be compared with the corresponding

differences between the true and the initial model parameters, which are shown in Figures 9, 11, 13, 15, 17, 19, and 21 respectively. Some observations can be made. Firstly, parameterizations with one velocity and two anisotropic parameters always give the best velocity estimates. NMO velocity, v_n, is best inverted using parameterization $\{v_n, \eta, \delta\}$ (Figure 14(a)), while horizontal velocity, v_h, is best resolved using $\{v_h, \epsilon, \eta\}$ (Figure 16(a)), and vertical velocity, v_z, is best resolved using parameterization $\{v_z, \epsilon, \delta\}$ (Figure 12(a)). However, the inverted velocity models show some unreal features that is a result of cross-talk from two anisotropic parameters within their parameterizations.

I also observe that parameterization $\{v_z, \epsilon, \delta\}$ also gives the best estimates in ϵ and δ (Figures 12(b) and 12(c) respectively). However, update in δ is very weak and contaminated by cross-talk from velocity. In fact, this is true for all parameterizations that include δ. Particularly, this cross-talk from velocity is so strong that δ is updated in the wrong direction in parameterizations $\{v_n, \eta, \delta\}$ (Figures 14(c)) and $\{v_n, v_h, \delta\}$ (Figure 20(c)). In terms of η, it is best resolved using parameterization $\{v_n, \eta, \delta\}$ (Figure 14(b)). However, the inverted η parameter is again degraded by cross-talk from velocity (NMO velocity, v_n, in this case), especially in the shallow part of the model. The inter-parameter cross-talk between velocity and anisotropic parameters is expected because the wide range of scattering angle over which velocity is resolvable overlap with those angles of anisotropic parameters (Gholami et al., 2013a).

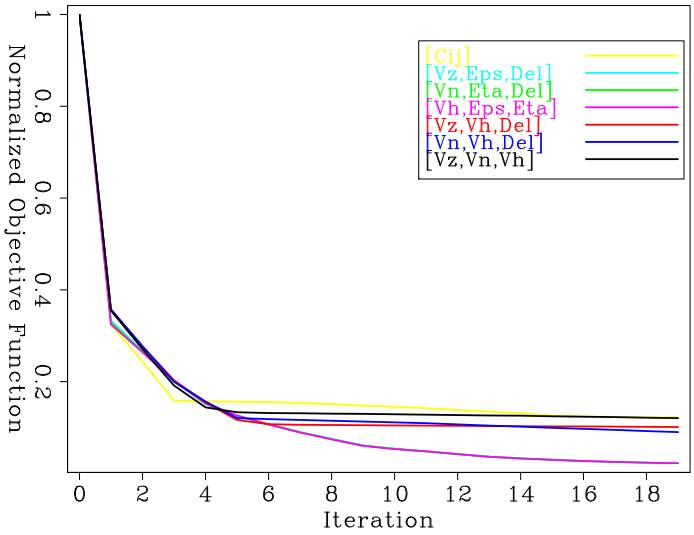

Figure 8: Comparison of objective functions from inversions with different parameterizations. Parameterizations with one velocity and two anisotropic parameters lead to the most reduced objective functions. [**CR**]

REGULARIZATION

Although acoustic anisotropic FWI has a smaller number of model parameters than its elastic equivalent, compared to isotropic FWI, its model space is still much larger. This results in a much bigger model null space, making the problem more ill-posed, and the inversion can more easily get stuck in local minima. One standard way to overcome this issue is to use regularization. The regularized objective function is

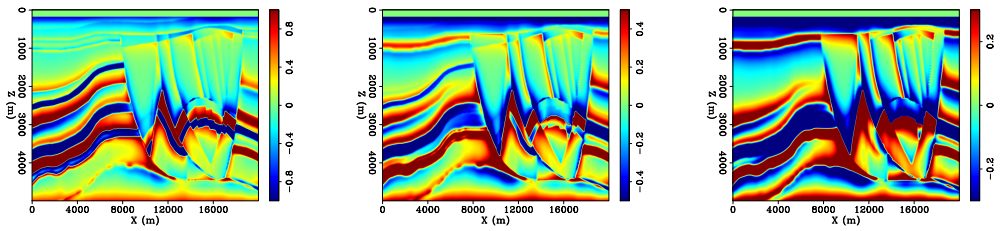

(a) (b) (c)

Figure 9: Differences between initial and true model: (a) c_{11}, (b) c_{13}, and (c) c_{33} in MPa. [**ER**]

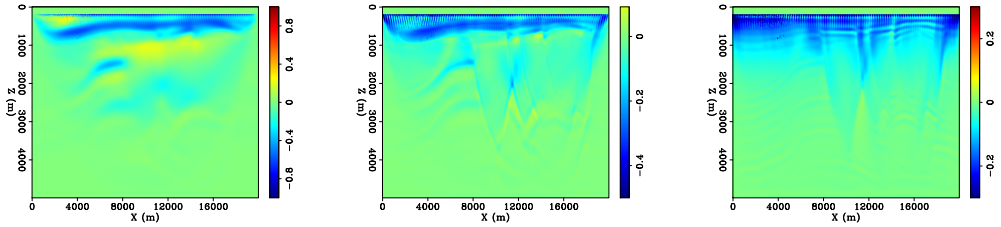

(a) (b) (c)

Figure 10: Updates after inversion: (a) c_{11}, (b) c_{13}, and (c) c_{33} in MPa. These updates are to be compared with the corresponding differences between true and initial model in Figure 9. [**CR**]

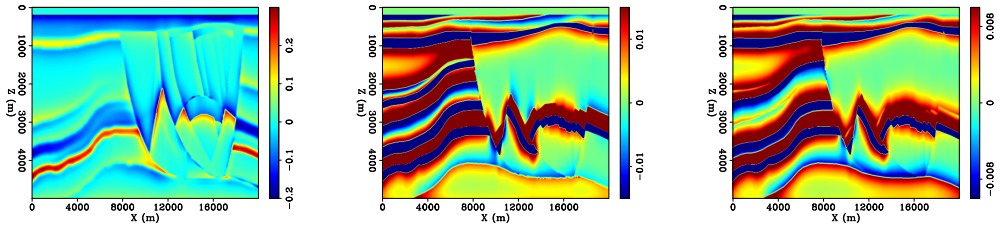

(a) (b) (c)

Figure 11: Differences between initial and true model: (a) v_z in km/s, (b) ϵ, and (c) δ. [**ER**]

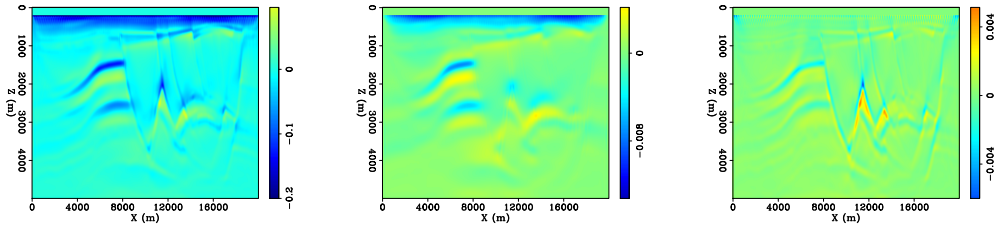

(a) (b) (c)

Figure 12: Updates after inversion: (a) v_z in km/s, (b) ϵ, and (c) δ. These updates are to be compared with the corresponding differences between true and initial model in Figure 11. This parameterization gives the best estimates in both velocity and anisotropic parameters. There is some cross-talk between velocity and the other two parameters, especially δ. [**CR**]

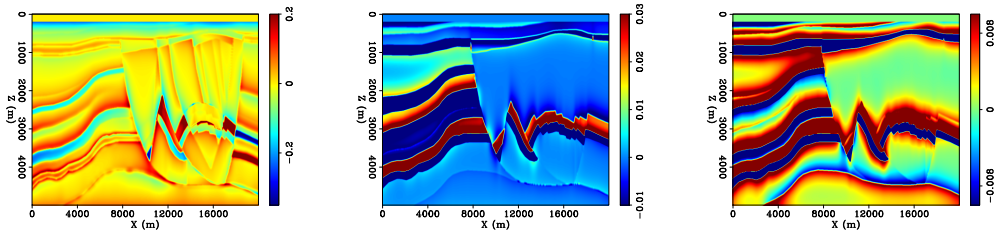

(a) (b) (c)

Figure 13: Differences between initial and true model: (a) v_n in km/s, (b) η, and (c) δ. [**ER**]

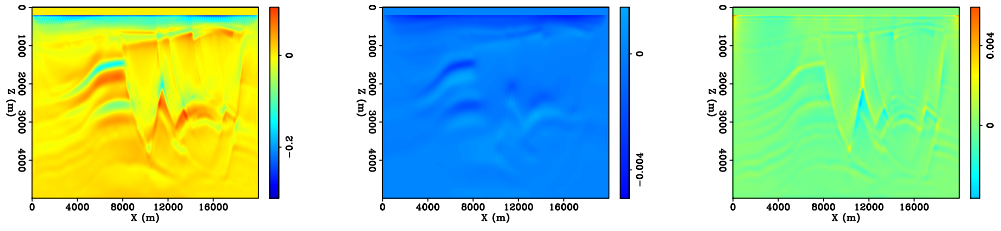

(a) (b) (c)

Figure 14: Updates after inversion: (a) v_n in km/s, (b) η, and (c) δ. These updates are to be compared with the corresponding differences between true and initial model in Figure 13. This parameterization gives the best estimates in v_n and η. Inverted models of theses two parameters also show some cross-talk. Cross-talk from v_n leads to wrong-direction update in δ. [**CR**]

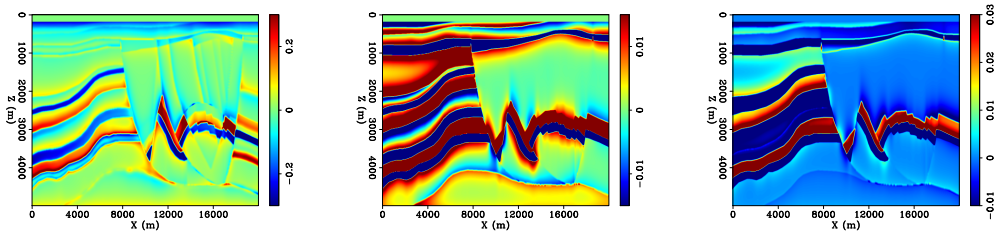

(a) (b) (c)

Figure 15: Differences between initial and true model: (a) v_h in km/s, (b) ϵ, and (c) η. [**ER**]

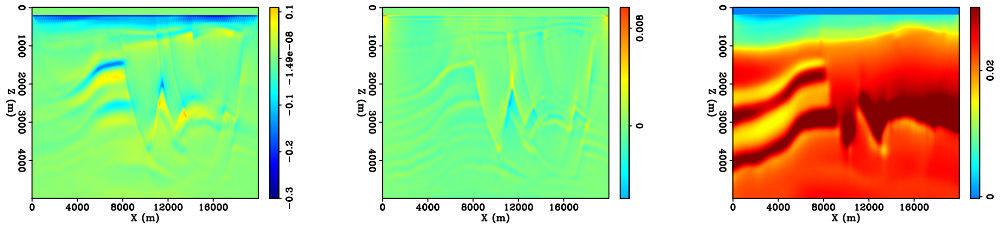

(a) (b) (c)

Figure 16: Updates after inversion: (a) v_h in km/s, (b) ϵ, and (c) η. These updates are to be compared with the corresponding differences between true and initial model in Figure 15. This parameterization gives the best estimate in v_h. ϵ update is contaminated by v_h. η is updated in the wrong direction. [**CR**]

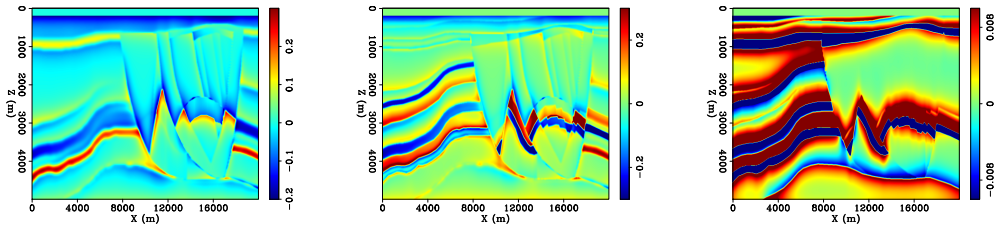

(a) (b) (c)

Figure 17: Differences between initial and true model: (a) v_z in km/s, (b) v_h in km/s, and (c) δ. [**ER**]

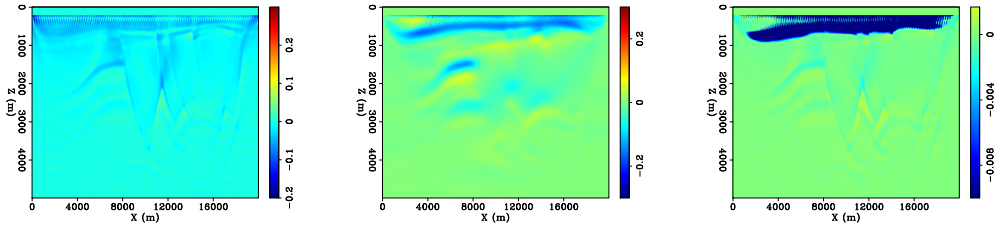

(a) (b) (c)

Figure 18: Updates after inversion: (a) v_z in km/s, (b) v_h in km/s, and (c) δ. These updates are to be compared with the corresponding differences between true and initial model in Figure 17. [**CR**]

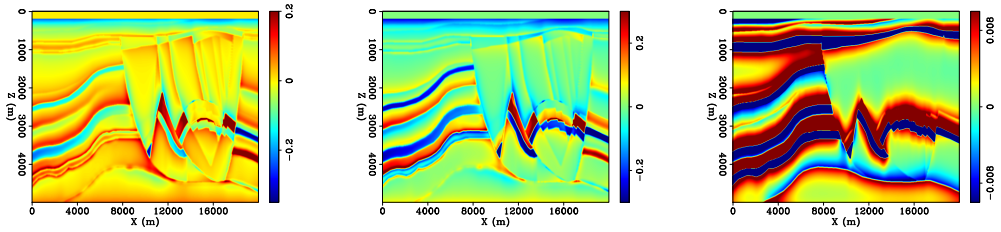

(a) (b) (c)

Figure 19: Differences between initial and true model: (a) v_n in km/s, (b) v_h in km/s, and (c) δ. [**ER**]

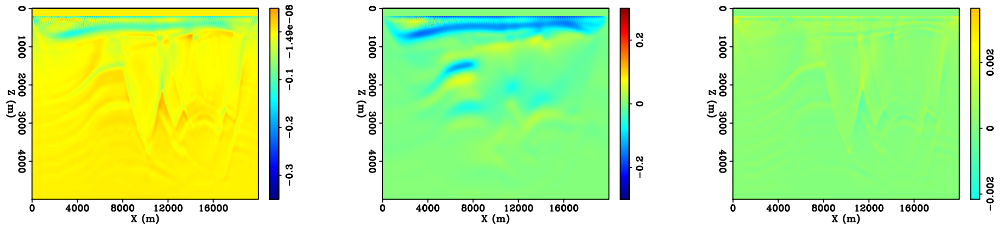

(a) (b) (c)

Figure 20: Updates after inversion: (a) v_n in km/s, (b) v_h in km/s, and (c) δ. These updates are to be compared with the corresponding differences between true and initial model in Figure 19. In some areas, δ is updated in the wrong direction due to cross-talk from velocities. [**CR**]

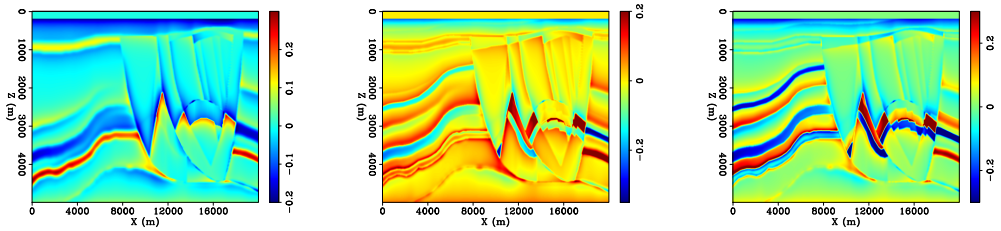

(a) (b) (c)

Figure 21: Differences between initial and true model: (a) v_z, (b) v_n, and (c) v_h in km/s. [**ER**]

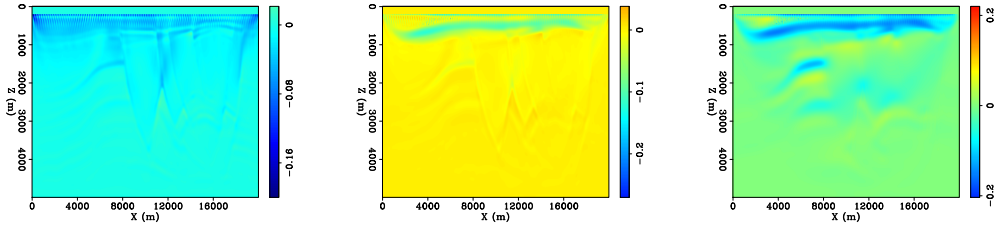

(a) (b) (c)

Figure 22: Updates after inversion: (a) v_z, (b) v_n, and (c) v_h in km/s. These updates are to be compared with the corresponding differences between true and initial model in Figure 21. [**CR**]

expressed as:

$$\chi(\mathbf{m}) = \frac{1}{2}\|d(\mathbf{x}_r, t; \mathbf{m}) - d_0(\mathbf{x}_r, t)\|_2^2 + \frac{\alpha}{2}\|\mathbf{Am}\|_2^2, \tag{10}$$

in which $\mathbf{A}$ is some styling operator that is related to the model covariance matrix. In the next example, I take this operator to be a steering filter obtained from the dip of the migrated image. Using a steering filter to spread dip information along geologic structures helps speed up convergence and improve inversion results. This was introduced and applied successfully to tomography by Clapp et al. (2004). Figure 23(a) shows the migrated image and Figure 23(b) shows the tangent of the dip angle, which is used to construct the steering filter $\mathbf{A}$. The inversion results with regularization are shown in Figure 24. This figure shows improvements in the inverted models compared to the non-regularized results (Figure 12). Dipping reflectors are more continuous and the inverted model parameters are closer to the true ones. Figure 25 shows that regularized inversion leads to a slightly lower objective function than without regularization. The improvements are, however, not very significant, which I suspect is due to the smooth dip field (Figure 23(b)). Moreover, cross-talk between velocity and anisotropic parameters is still present because the same steering filter is applied on all three parameters. Additional information (from rock physics, for example) can be used to obtain separate filters for individual parameters that can reduce their cross-talk.

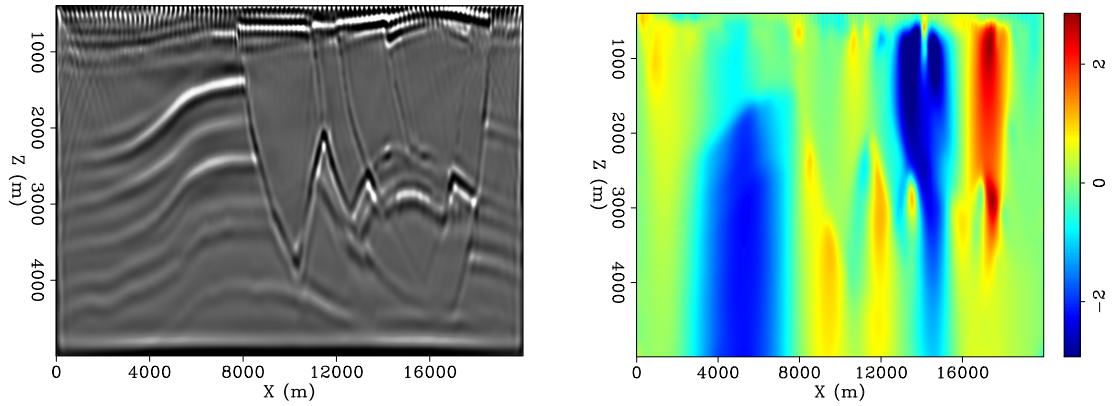

(a) (b)

Figure 23: (a) Migrated image and (b) dip (tangent of dip angle). [**CR**]

CONCLUSIONS

In this report I investigate three practical issues in anisotropic FWI. The first issue is how to account for differences in dimension, magnitude, and sensitivity among different parameters. I suggest applying a normalization which transforms the original parameters into a set of dimensionless parameters that more truly reflect their sensitivities. This normalization can be seen as a simple way to approximate the Hessian matrix. The second issue is parameterization. I have tested four types of parameterization: stiffness coefficients, one velocity with two anisotropic parameters, two

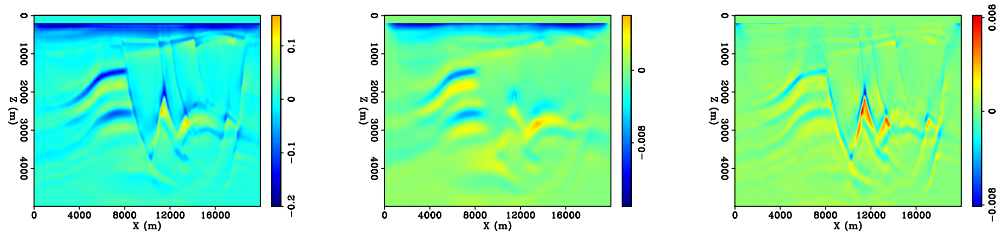

(a) (b) (c)

Figure 24: Updates after inversion with steering filter regularization: (a) v_z in km/s, (b) ϵ, and (c) δ. Inverted model parameters show more continuous dipping structures and better converge toward the true ones. Cross-talk is, however, still observable. [**CR**]

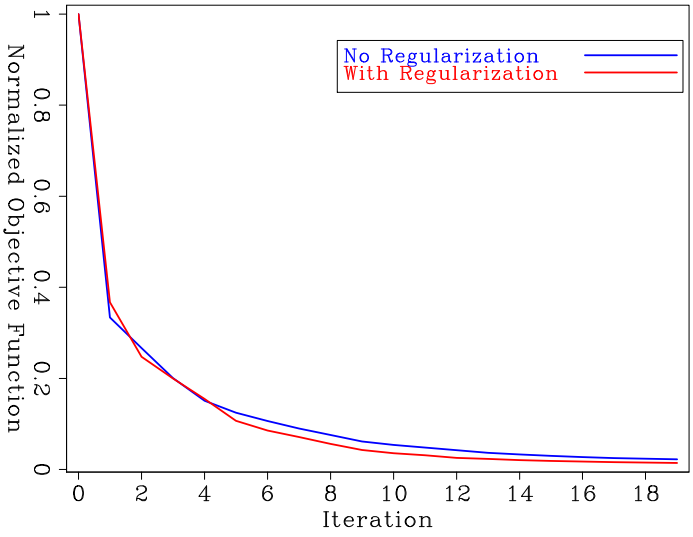

Figure 25: Comparison of objective functions from inversions with and without regularization. Regularization leads to a slightly lower objective function. [**CR**]

velocities with one anisotropic parameters, and three velocities. Performance of different parameterizations is evaluated by how much they reduce the objective function. I found that parameterizations with one velocity and two anisotropic parameters gave the best results. Especially, among all tested parameterizations, $\{v_z, \epsilon, \delta\}$ results in the best estimates in both vertical velocity and anisotropic parameters despite some cross-talk. Another issue in anisotropic FWI is the large model null space. I have shown that a regularization with a steering filter constructed using dip information from the migrated image can improve the results and lead to better inverted models. Additional information from rock physics can also be used for regularization and is the subject of my future work.

REFERENCES

Alkhalifah, T. and I. Tsvankin, 1995, Velocity analysis for transversely isotropic media: Geophysics, **60**, 1550–1566.

Barnes, C., M. Charara, and T. Tsuchiya, 2008, Feasibility study for an anisotropic full waveform inversion of crosswell seismic data: Geophysical Prospecting, **56**, 897–906.

Clapp, R. G., B. Biondi, and J. F. Claerbout, 2004, Incorporating geologic information into reflection tomography: Geophysics, **69**, 533–546.

Duveneck, E. and P. M. Bakker, 2011, Stable P-wave modeling for reverse-time migration in tilted TI media: Geophysics, **76**, No. 2, WA3–WA11.

Fichtner, A., 2011, Full seismic waveform modeling and inversion: Springer.

Gholami, Y., R. Brossier, S. Operto, A. Ribodetti, and J. Virieux, 2013a, Which parameterization is suitable for acoustic vertical transver isotropic full waveform inversion? Part 1: Sensitivity and trade-off analysis: Geophysics, **78**, No. 2, R81–R105.

———, 2013b, Which parameterization is suitable for acoustic vertical transver isotropic full waveform inversion? Part 2: Synthetic and real data case studies from Valhall: Geophysics, **78**, No. 2, R107–R124.

Le, H., 2016, Anisotropic full waveform inversion : SEP-Report, **163**, 155–162.

Lee, H.-Y., J. M. Koo, D.-J. Min, B.-D. Kwo, and H. S. Yoo, 2010, Frequency-domain elastic full waveform inversion for VTI media: Geophysical Journal International, **183**, 884–904.

Plessix, R. E. and Q. Cao, 2011, A parameterization study for surface seismic full waveform inversion in an acoustic vertical transversely isotropic medium: Geophysical Journal International, **185**, 539–556.

Thomsen, L., 21986, Weak elastic anisotropy: Geophysics, **51**, 1954–1966.

Warner, M., A. Ratcliffe, T. Nangoo, J. Morgan, A. Umpleby, N. Shah, V. Vinje, I. Stekl, L. Guasch, C. Win, G. Conroy, and A. Bertrand, 2013, Anisotropic 3D full-waveform inversion: Geophysics, **78**, No. 2, R59–R80.